



HAL
open science

Applying the Dempster–Shafer Fusion Theory to Combine Independent Land-Use Maps: A Case Study on the Mapping of Oil Palm Plantations in Sumatra, Indonesia

Carl Bethuel, Damien Arvor, Thomas Corpetti, Julia Hélie, Adrià Descals, David Gaveau, Cécile Chéron-Bessou, Jérémie Gignoux, Samuel Corgne

► To cite this version:

Carl Bethuel, Damien Arvor, Thomas Corpetti, Julia Hélie, Adrià Descals, et al.. Applying the Dempster–Shafer Fusion Theory to Combine Independent Land-Use Maps: A Case Study on the Mapping of Oil Palm Plantations in Sumatra, Indonesia. *Remote Sensing*, 2025, 17 (2), pp.234. 10.3390/rs17020234 . hal-04925106

HAL Id: hal-04925106

<https://hal.inrae.fr/hal-04925106v1>

Submitted on 1 Feb 2025

HAL is a multi-disciplinary open access archive for the deposit and dissemination of scientific research documents, whether they are published or not. The documents may come from teaching and research institutions in France or abroad, or from public or private research centers.



L'archive ouverte pluridisciplinaire **HAL**, est destinée au dépôt et à la diffusion de documents scientifiques de niveau recherche, publiés ou non, émanant des établissements d'enseignement et de recherche français ou étrangers, des laboratoires publics ou privés.



Distributed under a Creative Commons Attribution - NonCommercial 4.0 International License

Article

Applying the Dempster–Shafer Fusion Theory to Combine Independent Land-Use Maps: A Case Study on the Mapping of Oil Palm Plantations in Sumatra, Indonesia

Carl Bethuel ¹, Damien Arvor ^{1,*}, Thomas Corpetti ¹, Julia Hélie ², Adrià Descals ³, David Gaveau ⁴,
Cécile Chéron-Bessou ⁵, Jérémie Gignoux ⁶ and Samuel Corgne ¹

¹ CNRS (French National Center for Scientific Research), Université Rennes 2, LETG, UMR 6554, 35000 Rennes, France; carl.bethuel@univ-rennes2.fr (C.B.)

² PSE (Paris School of Economics), EHESS (School of Advanced Studies in the Social Sciences), UMR 8545, 48 boulevard Jourdan, 75014 Paris, France

³ CREAM (Center for Ecological Research and Forest Applications), Cerdanyola del Vallès, 08193 Barcelona, Spain

⁴ TheTreeMap, 46600 Martel, France

⁵ CIRAD (French Agricultural Research Center for International Development), UMR ABSys, Elsa Group, Av. Agropolis, 34398 Montpellier, France

⁶ PSE (Paris School of Economics), INRAE (French National Research Institute for Agriculture, Food and Environment), UMR 8545, 48 boulevard Jourdan, 75014 Paris, France; jeremie.gignoux@psemail.eu

* Correspondence: damien.arvor@univ-rennes2.fr

Abstract: The remote sensing community benefits from new sensors and easier access to Earth Observation data to frequently released new land-cover maps. The propagation of such independent and heterogeneous products offers promising perspectives for various scientific domains and for the implementation and monitoring of land-use policies. Yet, it may also confuse the end-users when it comes to identifying the most appropriate product to address their requirements. Data fusion methods can help to combine competing and/or complementary maps in order to capitalize on their strengths while overcoming their limitations. We assessed the potential of the Dempster–Shafer Theory (DST) to enhance oil palm mapping in Sumatra (Indonesia) by combining four land-cover maps, hereafter named DESCALS, IIASA, XU, and MAPBIOMAS, according to the first author’s name or the research group that published it. The application of DST relied on four steps: (1) a discernment framework, (2) the assignment of mass functions, (3) the DST fusion rule, and (4) the DST decision rule. Our results showed that the DST decision map achieved significantly higher accuracy ($Kappa = 0.78$) than the most accurate input product ($Kappa = 0.724$). The best result was reached by considering the probabilities of pixels to belong to the OP class associated with DESCALS map. In addition, the belief (i.e., confidence) and conflict (i.e., uncertainty) maps produced by DST evidenced that industrial plantations were detected with higher confidence than smallholder plantations. Consequently, Kappa values computed locally were lower in areas dominated by smallholder plantations. Combining land-use products with DST contributes to producing state-of-the-art maps and continuous information for enhanced land-cover analysis.

Keywords: data fusion; Dempster–Shafer theory; oil palm mapping; Indonesia



Academic Editor: Andrea Garzelli

Received: 9 December 2024

Revised: 30 December 2024

Accepted: 7 January 2025

Published: 10 January 2025

Citation: Bethuel, C.; Arvor, D.; Corpetti, T.; Hélie, J.; Descals, A.; Gaveau, D.; Chéron-Bessou, C.; Gignoux, J.; Corgne, S. Applying the Dempster–Shafer Fusion Theory to Combine Independent Land-Use Maps: A Case Study on the Mapping of Oil Palm Plantations in Sumatra, Indonesia. *Remote Sens.* **2025**, *17*, 234. <https://doi.org/10.3390/rs17020234>

Copyright: © 2025 by the authors. Licensee MDPI, Basel, Switzerland. This article is an open access article distributed under the terms and conditions of the Creative Commons Attribution (CC BY) license (<https://creativecommons.org/licenses/by/4.0/>).

1. Introduction

Remote sensing (RS) science is essential for producing spatio-temporal indicators to monitor and understand human activities and their environmental impacts. To do so,

RS scientists benefit from the continuous development of new remote sensors and easier access to Earth Observation (EO) data. In addition, cloud computing technologies offer new perspectives to process large and complex datasets (Google Earth Engine (GEE) [1], or EO data cubes [2]). These solutions represent a major evolution, and their wide adoption results in the frequent release of new global and regional products for the mapping of land cover and land-use dynamics [3,4]. Global maps of forest cover and degradation [5,6], water surfaces [7], mangroves [8], or land cover [9] are seminal examples of such initiatives. These are completed by regional and national efforts such as land-cover mapping in France [10] and Brazil [11], cropland mapping in East Asia [12], forest and mangroves monitoring in Southeastern Asia [13,14], or tree plantations in China [15,16].

However, while such products undoubtedly improve our ability to monitor regional and global land-use/cover dynamics, their propagation can also confuse end-users when it comes to identifying the maps that best meet their requirements. More precisely, the proliferation of heterogeneous land-use/cover maps relying on different data (e.g., optical and/or radar imagery at different spatial resolutions), mapping methods (e.g., supervised vs. unsupervised classifications), and validation strategies (e.g., different validation indices or sampling design) raises new issues and opportunities for the RS community. In this regard, a major issue concerns the real potential of such a diversity of large-scale land-use/cover products to support the implementation and monitoring of environmental policies. As a seminal example to illustrate this point, the Food and Agriculture Organization of the United Nations (FAO) has recently developed an open access digital platform to monitor the implementation of the European Union Deforestation Regulation (EUDR [17]) based on various global forest monitoring products. This platform, named Whisp (“What is in that plot?” [18]), relies on a “convergence of evidence” approach that is built on the hypothesis that “no single definitive source of geospatial data can tell the whole story around any given plot of land; rather, various existing datasets contribute to understanding what has most probably occurred at that location and support to lessen the impact of individual biases or errors present in any single piece of evidence or data source” [18].

In this context, data fusion methods combining heterogeneous information offer promising expectations to reach optimized state-of-the-art maps. Indeed, data fusion refers to: “the joint use of heterogeneous information for decision support” [19]. There are actually various ways to categorize data fusion methods. Dasarathy [20] and Benediktsson and Sveinsson [21] classify methods depending on input and output data types. At the data level (also named low-level fusion), data fusion combines raw data (e.g., spectral reflectances in remote sensing images, [22,23]) to produce new data (e.g., spectral reflectances at a higher spatial or spectral resolution). At the feature level (also named mid-level fusion), data fusion combines extracted features (e.g., texture, shape, spectral indices or features issued from deep neural networks) to generate richer representations or inputs for classification and modeling. Finally, at a high level (also named {late/information/decision}-fusion), data fusion combines already-processed information (e.g., classified maps) to support decision making [24,25].

In this study, as raw and derived data are not available for all sources, unlike classified ones, we rely on late-fusion approaches. Such methods can be broadly categorized into three main types: (i) voting-based methods that aggregate decisions from multiple sources, using strategies such as majority voting, weighted voting (assigning reliability weights), or ranked voting based on the importance of each source [26]; (ii) rule-based methods that combine information through predefined logical rules or more flexible approaches like fuzzy logic to handle uncertainty [27–29] and (iii) probabilistic methods that model uncertainties explicitly, leveraging techniques such as Bayesian inference, naive Bayes classifiers (assuming source independence), or the Dempster–Shafer Theory (DST) for

belief-based reasoning. These approaches ensure robust decision-making by integrating diverse outputs effectively [30,31].

In this context, the DST presents interesting assets to manage uncertainties and deal with numerous independent sources through the concept of mass functions. DST, first developed by A. Dempster in 1967 [32] and later extended by G. Shafer in 1976 [33], generalizes the Bayesian theory of probability. Unlike classical probability, which requires precise probabilities for all possible outcomes, the Dempster–Shafer theory allows for uncertainty by assigning belief masses to sets of possibilities rather than individual events. The belief function quantifies the support for a proposition, while the plausibility function measures how much the evidence does not refute it. Evidence from different sources is combined using Dempster’s rule of combination, which updates beliefs by merging compatible information and redistributing conflict proportionally. This flexibility makes the approach particularly useful in situations with incomplete or uncertain data. Indeed, DST provides a robust analysis by not interpreting the lack of information as evidence against an assumption [34]. In addition, DST is both commutative and associative (i.e., the order of using sources does not impact the result), ensuring the infinite integration of evidences as long as the input sources are independent. However, DST also has limitations, such as the complex assignment of belief mass functions [30] and shortcomings in the case of highly contradictory evidence [35].

Several studies successfully applied DST for land cover [34,36–39], forest [40] and urban [41]) monitoring, or to estimate precipitation [42]. However, these studies also showed a few limitations: (1) they were restricted to small-scale applications or to low resolution data fusion; (2) belief mass functions are generally based on literature reviews and expert knowledge; and (3) conflict redistribution was not optimized to efficiently deal with contradictory evidences. Therefore, the frequent publication of large-scale maps at high or moderate resolutions (10 to 30 m) associated (sometimes) with pixel-level quality indices promotes new opportunities and challenges for the large-scale operational application of DST in the era of Big Earth Observation (Big EO) data.

In the present study, we assess the potential of DST to combine various heterogeneous independent land-use maps. As a case study, we focus on the mapping of oil palm (OP) plantations in Sumatra island, Indonesia. This application is particularly relevant because (1) OP expansion is known as a major driver of deforestation, (2) the RS community has recently released various heterogeneous and independent OP maps, and (3) mapping OP plantations is very challenging due to the complex discrimination between OP plantations, forests, and other tree plantations, so there is an urgent need to increase map accuracy, especially in view of the future implementation of the EUDR.

2. Study Case

Oil palm (*Elæis guineensis* Jacq.) is the most cultivated oilseed in the world due to its high average yields. OP plantations are spread over 45 tropical countries [43], with a special emphasis on Indonesia (about 60% of the world production). Here, we focus on Sumatra island (a total area of 473,481 km²), which is home to the largest OP areas in Indonesia (e.g., 9 million ha in Sumatra in 2019 vs. 6 million ha in Kalimantan [44]) (Figure 1). OP cultivation in Indonesia was initiated in the province of North Sumatra in the 1900s [45], then spread to the whole island during a major expansion phase supported by public transmigration policies in the 1980s, and was finally continued by the privatization of the oilseed sector in the 1990s [46].

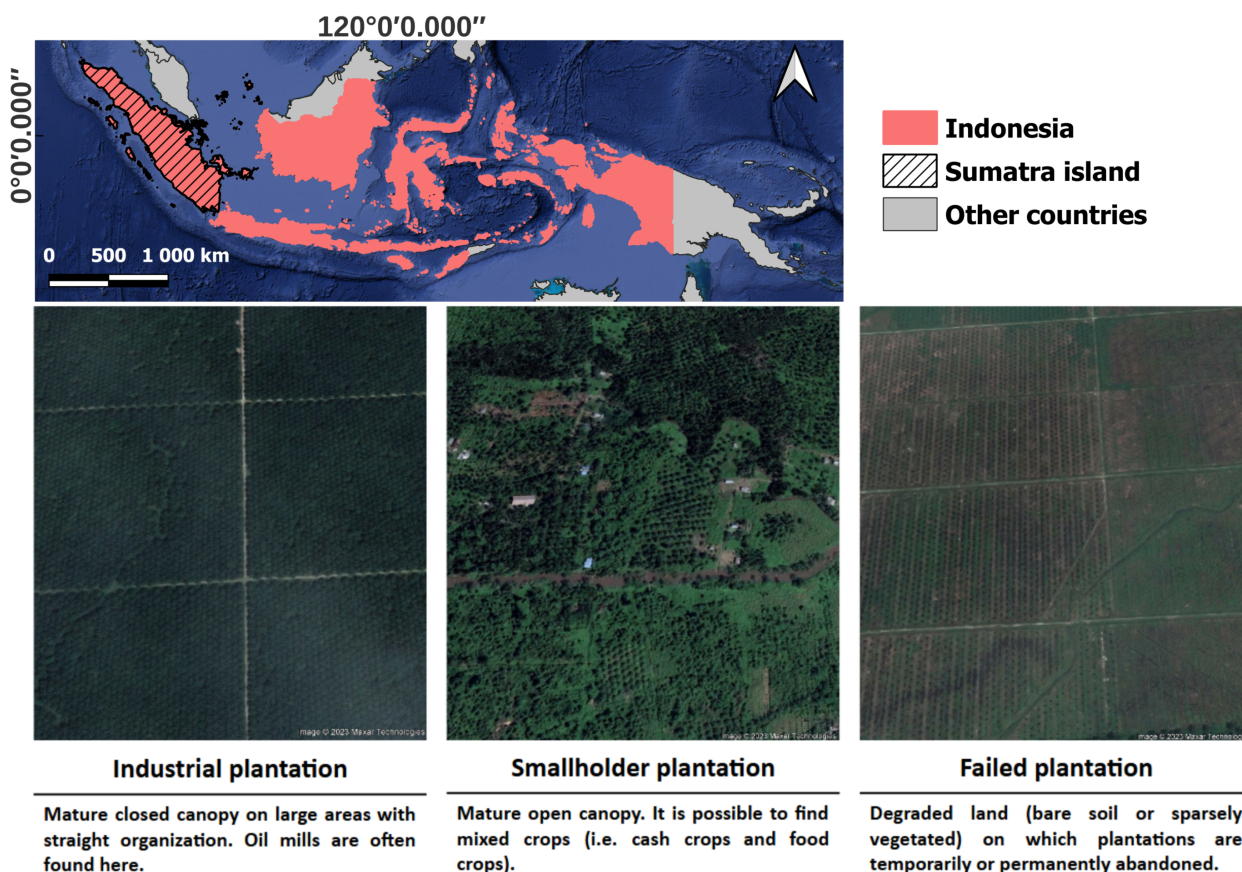


Figure 1. Location of the study area, Sumatra island (Indonesia), and illustration of different types of oil palm plantations as seen from very-high-resolution remote sensing image (© Google Earth).

Whereas OP expansion is a pillar of socio-economic development in Indonesia, important socio-environmental concerns have drawn the attention of the civil society and the scientific community, especially regarding the deforestation of primary forests and peat swamps with drainage and fire [46]). Such high deforestation rates contribute to high greenhouse gas emissions in Indonesia [47] and dramatically impact the climate. In addition, Indonesia is a biodiversity hot-spot with endemic and symbolic species severely impacted by OP expansion [48]. Intensive OP plantations also affect the environment through the pollution of soil and water resources due to synthetic fertilizers or pesticides [49]. Finally, OP expansion was also criticized for exacerbating social conflicts over land rights with native peoples and for contributing to social inequities [50,51].

Addressing these numerous socio-environmental issues requires the efficient mapping of OP plantations in Indonesia. However, remote sensing-based OP mapping is a very challenging task. On the one hand, optical data suffer from high cloud-cover rates that prevent accurate single-date mapping but benefit from long historic datasets to monitor inter-annual dynamics and derive important information such as the age of plantations [52–56]. In this regard, Landsat (since the 1980s) [54–56] and MODIS (since the 2000s) [53,57] images have been commonly used to monitor the expansion of OP plantations due to their long temporal continuity, whereas maps with finer spatial resolutions were only recently produced using Sentinel-2 images [58,59].

On the other hand, radar images such as ALOS-PALSAR and ALOS-PALSAR2 data in the L-band [60–62] or Sentinel-1 data in the C-band [58,63] are less affected by cloud cover and more suitable for detecting palm trees, especially in closed-canopy plantations [59,64]. However, the short temporal archive hinders the inter-annual monitoring of OP expansion [60,62–64]. As a logical continuation, recent studies explored the synergy

between optical and radar images [16] to exploit the advantages of each data point and improve both single-date mapping [58,61,65] and inter-annual monitoring [66,67].

Last but not least, beyond the data and methodological issues, it is also worth noting that OP mapping efforts are also affected by semantic concerns. Indeed, since OP is a perennial crop with a >25-year life cycle, some mapping efforts may only focus on mature plantations (>3 years), while others also include young plantations [52,55,56]. In addition, failed plantations (Figure 1) (i.e., abandoned plantings due to financial reasons or palm diseases) are usually ignored. Finally, OP plantations often implicitly focus on large “industrial plantations” in organized landscapes (Figure 1) and tend to disregard “smallholder plantations”, which still actually represent about 40% of OP plantations in Indonesia.

3. Data

The present study relies on five maps of OP plantations (Figure 2), hereafter named GAVEAU, DESCALS, XU, IIASA, and MAPBIOMAS, based on the first author’s name or the research group that published it (Table 1). The first map (GAVEAU) is here considered as a reference dataset because it was produced through visual photo-interpretation, relying on trained human expertise assumed to be the best available recognition method to date [68]. The four other maps are RS-based classifications and are considered as input sources to the data fusion approach. These four maps were chosen as they were freely available, achieving high accuracy levels and high heterogeneity, since they rely on different data, methods, and definitions of OP plantations.

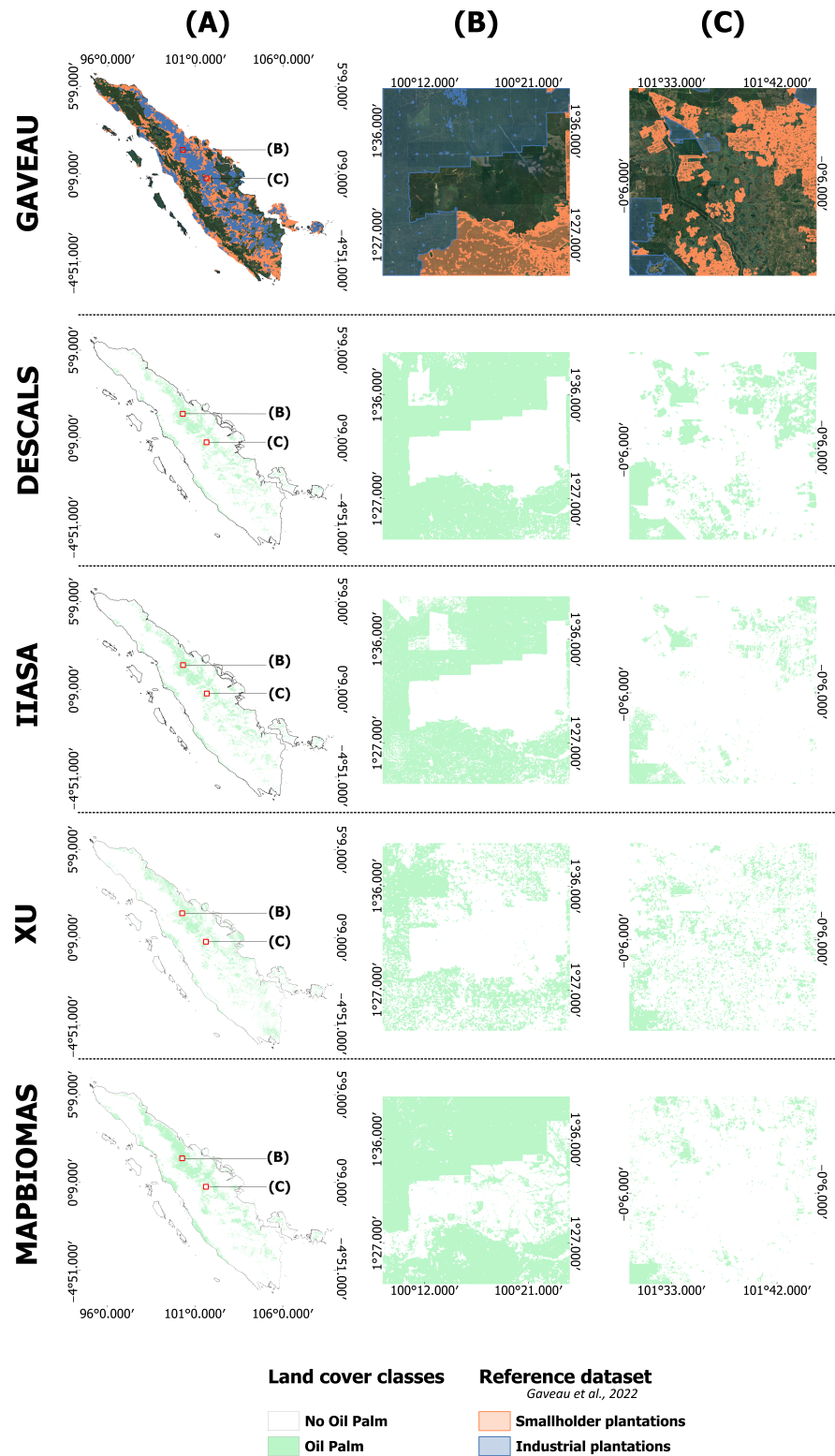


Figure 2. Presentation of the reference (GAVEAU [44]) and input land-use maps at Sumatra-scale (A) and tile-scale, considering a tile dominated by industrial plantations (B) and a tile dominated by smallholder plantations (C).

Table 1. The characteristics of the reference dataset and input sources.

Map Name	Type	Year Map	Data (Optical/Radar)	Spatial Resolution	Methods	Land-Cover Classes	Accuracy	Citation
GAVEAU	REF	2019	Landsat & SPOT-6/ -	1/50,000	Visual interpretation	Industrial Smallholder Other	OA = 95.6%	Gaveau et al. [44]
DESCALS	CLASSIF	2019	Sentinel-2 / Sentinel-1	10 m	Deep Learning	Industrial Smallholder Other	OA = 94.02%	Descals et al. [59]
IIASA	CLASSIF	2017	Landsat/ Sentinel-1	30 m	Unsupervised classification	No Oil Palm Oil Palm	OA = 84.83%	Danylo et al. [69]
XU	CLASSIF	2016	MODIS/ ALOS-PALSAR	100 m	Random Forest	No Oil Palm Oil Palm	F1-score = 0.72	Xu et al. [57]
MAPBIOMAS	CLASSIF	2019	Landsat/ -	30 m	Random Forest	Oil Palm + 7 other land cover classes	/	Mapbiomas [70]

3.1. GAVEAU Map (Reference)

The reference map (Figure 2) was published by Gaveau et al. [44] and aims to map land conversion to OP for both plantation types (i.e., industrial vs. smallholder plantations) with a two-step approach.

First, annual Landsat median composites were produced and visually interpreted between 2000 and 2019 to map industrial plantations. Second, smallholder plantations were mapped by the visual interpretation of SPOT-6 images at 1.5 m spatial resolution for 2016. The map was produced by the AURIGA non-governmental organization and approved by the Indonesian government. The map of 2016 was updated until 2019 through change detection techniques using Sentinel-1 composites, whereas the Tree Loss product [5] was used to estimate the planting years up to 2000. These annual maps were validated by the visual interpretation of very high resolution images on GEE (Overall Accuracy (OA) = 95.6% for 2019).

Based on this reference map, we created a stratified reference sample (hereafter named the GAVEAU sample). To do so, we divided Sumatra island into 723 tiles (one tile \approx 900 km²). For each tile, we randomly selected 2500 reference points (except for tiles with small land areas) and split them according to the proportion of each land-use class (i.e., oil palm (OP), no oil palm (NOP)) in line with the stratified sampling design proposed by Olofsson et al. [71]. We thus created a large dataset of 1,804,989 points (1,540,483 points for NOP vs. 264,506 points for OP), further divided into training (70%, i.e., 1,263,448 points) and test (30%, i.e., 541,541 points) samples.

3.2. DESCALS Map (Input Source 1)

Descals et al. [59] mapped mature closed-canopy OP plantations for 2019 at a global scale. First, potential areas for OP plantations were identified with climate features (WorldClim V1 Bioclim data) and an existing map of industrial OP plantations. Second, a deep learning classification model (convolutional neural networks) was trained with Sentinel-1 IW GRD and Sentinel-2 L2A data for the second half of 2019 at a 10 m spatial resolution. The results showed an OA = 94.02% for Sumatra (Figure 2), with smallholder plantations showing lower user accuracy (63.27% vs. 89.25%) and higher producer accuracy (81.44% vs. 69.15%) than industrial plantations.

3.3. IIASA Map (Input Source 2)

Danylo et al. [69] mapped the extent and age of OP plantations in Southeast Asia through a two-step method. First, the OP extent map was obtained for 2017 with a Sentinel-1 IW GRD annual composite in dual-polarization VV and VH at 30 m spatial resolution. An unsupervised classification by majority voting was computed with the VV band, VH band, VV/VH ratio, and texture metrics from the gray-level co-occurrence matrix.

Second, the age of OP plantations was estimated by detecting the year of the most recent high values of the Bare Soil Index [72] in the Landsat time series since 1984. The OP map for Sumatra (Figure 2) in 2017 was validated (OA = 84.83%) with a dataset produced by a collaborative visual interpretation for 8,609 random sites.

3.4. XU Map (Input Source 3)

Xu et al. [57] produced annual maps of OP plantations for Malaysia and Indonesia between 2001 and 2016 with a two-step approach. First, binary maps (OP/NOP) were produced for six years (2007 to 2010, 2015, and 2016) by computing a random forest integrating four variables (HH band, HV band, HH-HV difference, and HH/HV ratio) derived from L-band ALOS PALSAR and ALOS PALSAR-2 data, which were previously resampled from 25 m to 100 m to smooth the inherent noise in radar data.

Second, a BFAST change detection algorithm [73] was applied to the MODIS NDVI time series (resampled from 250 m to 100 m spatial resolution) to fill in the missing years in the ALOS-PALSAR and ALOS-PALSAR2 data (between 2011 and 2014). The map was validated with an F-score of 0.72 in 2016 for Sumatra (Figure 2).

3.5. MAPBIOMAS Map (Input Source 4)

The MAPBIOMAS product (Figure 2) was released in 2022 [70]. In line with the MapBiomas Brazil initiative, it relies on optical data to produce national-scale annual land-use maps between 2000 and 2019 at a 30 m spatial resolution. Unlike other maps, OP plantations were not the unique target class, but were mapped due to their importance for environmental dynamics in Indonesia. Time series of the Landsat 5, 7, and 8 images of the dry season period (April to September) were processed on GEE to compute spectral indices and soil fractions. Statistical metrics were then applied to summarize the temporal information in composite images then classified with a random forest algorithm using a training sample obtained through visual interpretation. Although the annual cloud-free classifications are freely available online, the validation process has not yet been finalized.

4. Methods

4.1. Introduction to the Dempster-Shafer Theory

The data fusion relies on the DST, which is a mathematical framework for modeling and reasoning under uncertainty using measures of plausibility and belief. The DST combines “evidence sources” into four major stages (Figure 3).

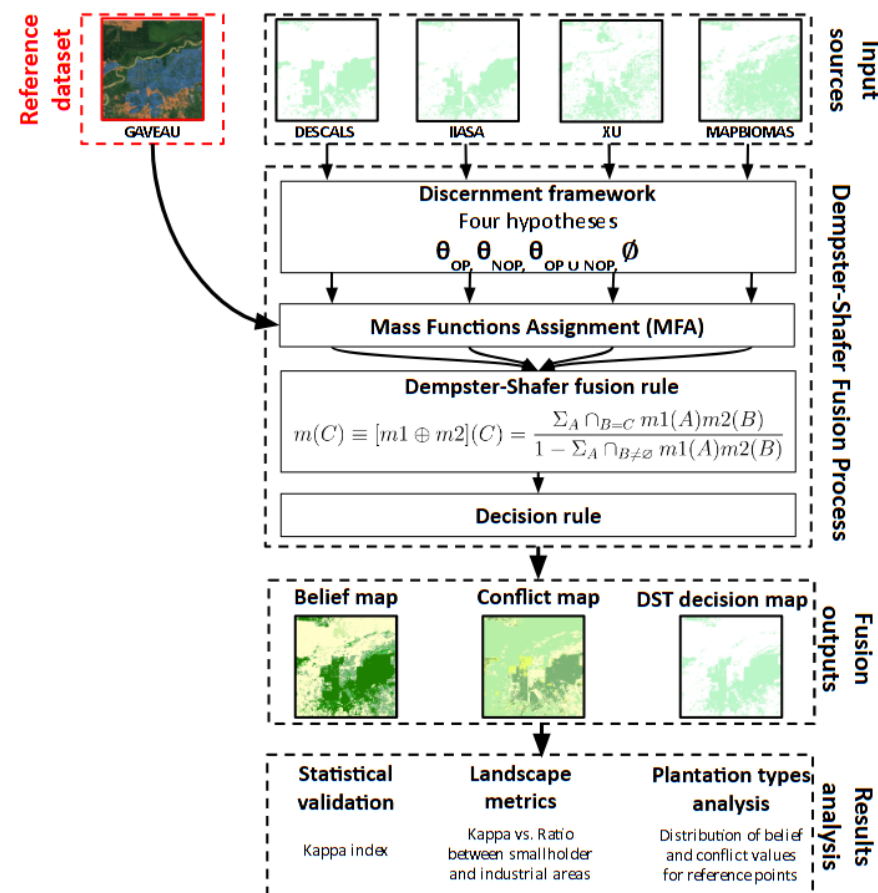


Figure 3. A flowchart of the methodology, including input sources, stages of DST fusion process, outputs, and validation approach.

1. **The discernment framework (DF)** sets the hypothesis of the fusion process, i.e., it defines all the possible classes (including uncertain ones) potentially assigned to a pixel.
2. **The Mass Functions Assignment (MFA)** determines the belief level associated with each element of the discernment framework. For each each input source, it assigns numeric mass functions for each pixel and each element of the DF.
3. **The Dempster–Shafer fusion rule** (symbolized by \oplus) combines the mass functions to estimate the belief and the plausibility for each pixel for each hypothesis.
4. **The decision rule (DR)** relies on these metrics to assign a hypothesis to each pixel, i.e., to assign a final decision to each pixel.

4.1.1. Definition of the Discernment Framework

The discernment framework (noted Θ) is composed of the set of possible classes θ (also called singletons) and all uncertainties between classes, i.e., all possible unions over them (Equation (1)). Since the OP class is the only common class among the four input sources, we focused on OP vs. NOP mapping. As a consequence, the discernment framework is composed of four hypotheses: oil palm (θ_{OP}), no oil palm (θ_{NOP}) the union of OP and NOP ($\theta_{OP} \cup \theta_{NOP}$), i.e., uncertainty between these two hypothesis, and the empty set \emptyset showing that there are no other hypotheses (Figure 4).

$$\Theta = \{\theta_1, \theta_2, \dots, \theta_n, \theta_1 \cup \theta_2, \dots, \theta_1 \cup \theta_n, \theta_1 \cup \theta_2 \cup \theta_3, \dots, \theta_1 \cup \dots \cup \theta_n\} \quad (1)$$

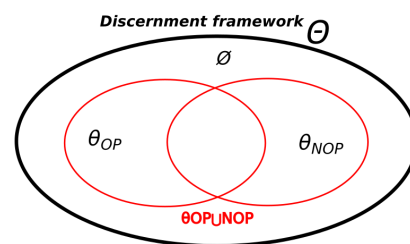


Figure 4. The discernment framework is composed of the empty set \emptyset , the oil palm class θ_{OP} , the no oil palm class θ_{NOP} , and the union of OP and NOP $\theta_{OP} \cup \theta_{NOP}$, representing the uncertainty.

Setting the discernment framework implies that the four heterogeneous input sources share similar characteristics, i.e., the same spatial resolution and land-use classes. For this reason, all inputs maps were (1) resampled at 10 m spatial resolution (i.e., the resolution of the finest input map from DESCALS) with the nearest neighbor method and (2) reclassified into two classes (OP and NOP).

4.1.2. The Mass Functions Assignment (MFA)

The MFA intends to assign masses for each element of the discernment framework ($\theta_{OP}, \theta_{NOP}, \theta_{OP \cup NOP}, \emptyset$) that must respect the following rules:

$$m(\theta) \in [0, 1]; \sum_{\theta \in \Theta} m(\theta) = 1; m(\emptyset) = 0 \quad (2)$$

In other words, at MFA stage, we define the mass function m for a pixel to be classified as OP (element θ_{OP}) or NOP (element θ_{NOP}), and we also assign a mass to the uncertainty (element $\theta_{OP} \cup \theta_{NOP}$). Ideally, these masses should rely on pixel-level probabilities associated with each input map. However, such probabilities were only released for the DESCALS map. We thus proposed an original approach based on the accuracy indices to set the mass functions for all input maps (although the initial DESCALS probabilities were also used—see Section 4.2).

To do so, we validated the accuracy of all sources with the GAVEAU reference training sample, relying on the error matrix and the Kappa index (K_p) to define the mass functions at the class level (Figure 5). One can rely on the overall uncertainty of different sources with respect to the validation map. Thus, if the classification is perfect ($K_p = 1$), we have complete confidence when predicting hypothesis θ_{OP} or θ_{NOP} , and under this ideal situation, one would have a generic mass distribution m as:

$$m_{OP}(\theta_{OP}) = 1 ; m_{OP}(\theta_{NOP}) = 0 ; m_{OP}(\theta_{OP} \cup \theta_{NOP}) = 0 ; m_{OP}(\emptyset) = 0$$

$$m_{NOP}(\theta_{OP}) = 0 ; m_{NOP}(\theta_{NOP}) = 1 ; m_{NOP}(\theta_{OP} \cup \theta_{NOP}) = 0 ; m_{NOP}(\emptyset) = 0$$

where m_{OP} (resp. m_{NOP}) stands for the situation where the classification issued from the source gave the class OP (resp. NOP).

If at this point the accuracy of the source is not perfect, this implies a lower confidence in the classification, i.e., $m_{OP}(\theta_{OP}) < 1$ and $m_{NOP}(\theta_{NOP}) < 1$. Therefore, a non-null value for the associated uncertainty $\theta_{OP} \cup \theta_{NOP}$ will be set. A rational choice to fix this uncertainty is to rely on the Kappa value, K_p , for each source. We then assign the global confidence as $m_{OP}(\theta_{OP}) = K_p$ (resp. $m_{NOP}(\theta_{NOP}) = K_p$). The fraction of false positives (resp. of false negatives) over points classified as OP (resp. NOP) can then be used to distribute the remaining mass $(1 - K_p)$ in $m_{OP}(\theta_{NOP})$ (resp. in $m_{NOP}(\theta_{OP})$). This leads to the following rule:

$$m_{OP}(\theta_{NOP}) = (1 - K_p) \frac{F_{op}}{F_{op} + T_{op}}$$

$$m_{NOP}(\theta_{OP}) = (1 - K_p) \frac{F_{nop}}{F_{nop} + T_{nop}}$$
(3)

with F_{op} (resp. F_{nop}) the number of false positives (resp. false negative), i.e., the number of points incorrectly classified as OP (resp. as NOP), and $F_{op} + T_{op}$ (resp. $F_{nop} + T_{nop}$) the total number of points classified as OP (resp. NOP). Here, F and T stand for *False* and *True* classification.

Lastly, the remaining mass is associated with the global uncertainty :

$$m_{OP}(\theta_{OP} \cup \theta_{NOP}) = 1 - K_p - (1 - K_p) \frac{F_{op}}{F_{op} + T_{op}}$$

$$m_{NOP}(\theta_{OP} \cup \theta_{NOP}) = 1 - K_p - (1 - K_p) \frac{F_{nop}}{F_{nop} + T_{nop}}$$
(4)

An illustration of mass functions assignment is given in Figure 5.

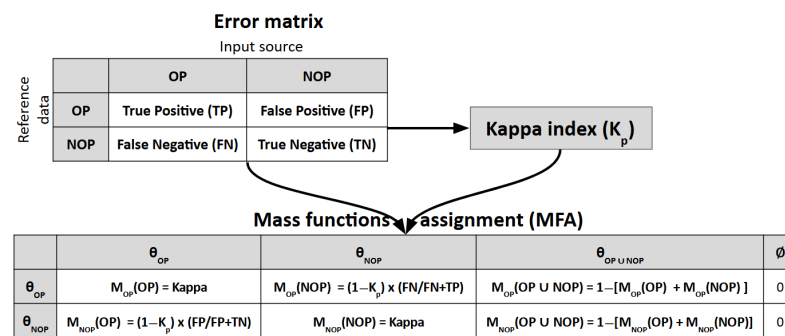


Figure 5. Mass functions assignment with an application to DESCALS map.

4.1.3. Dempster–Shafer Fusion Rule

The Dempster–Shafer fusion rule combines the mass functions assigned to each input source to estimate the belief and the plausibility for each hypothesis defined in the DF and is divided in two parts:

1. The numerator: the sum of the products between the MFA of each singleton (Equation (5)).
2. The denominator: the normalized coefficient, K_c (not to be confused with Kappa index, Kp) which refers to the conflict between input sources for one hypothesis (Equation (6)).

$$m(\theta_i) \equiv [S1 \oplus S2](\theta_i) = \frac{\sum_{\theta_j \cap \theta_l = \theta_i} m1(\theta_j)m2(\theta_l)}{K_c} \quad (5)$$

$$K_c = 1 - \sum_{\theta_j \cap \theta_l \neq \emptyset} m1(\theta_j)m2(\theta_l) \quad (6)$$

where m_1 and m_2 are mass functions of the evidence sources S_1 and S_2 defined in the DF Θ , and their purpose elements are θ_j and θ_l . $\sum_{\theta_j \cap \theta_l}$ represents the sum of all singletons $\theta_j, \theta_l \subseteq \Theta$ such as $\theta_j \cap \theta_l = \theta_i$. The coefficient K_c represents the conflict between the input sources and ranges from 0 (complete disagreement between sources) to 1 (complete agreement between sources).

For a better understanding, the example below (Application 1) details the application of DST for a random pixel with fictive values for two evidence sources ($m1$ and $m2$):

Application 1. Dempster–Shafer fusion rule with fictive values for two evidence sources ($m1$ and $m2$).

$$\begin{aligned} m1_{OP} &= 0.60 & m2_{OP} &= 0.5 \\ m1_{NOP} &= 0.33 & m2_{NOP} &= 0.4 \\ m1_{OP \cup NOP} &= 0.07 & m2_{OP \cup NOP} &= 0.1 \end{aligned} \quad (7)$$

$$\begin{aligned} K_c &= 1 - [m1_{OP}m2_{NOP} + m1_{NOP}m2_{OP}] \\ &= 0.595 \end{aligned} \quad (8)$$

$$\begin{aligned} Belief_{OP} &= \frac{m1_{OP}m2_{OP} + m2_{OP}m1_{OP \cup NOP} + m1_{OP}m2_{OP \cup NOP}}{K_c} \\ &= \frac{0.3 + 0.035 + 0.06}{0.595} \\ &= 0.664 \end{aligned} \quad (9)$$

$$\begin{aligned} Belief_{NOP} &= \frac{m1_{NOP}m2_{NOP} + m2_{NOP}m1_{OP \cup NOP} + m1_{NOP}m2_{OP \cup NOP}}{K_c} \\ &= \frac{0.132 + 0.028 + 0.033}{0.595} \\ &= 0.324 \end{aligned} \quad (10)$$

$$\begin{aligned} Belief_{OP \cup NOP} &= \frac{m1_{OP \cup NOP}m2_{OP \cup NOP}}{K_c} \\ &= \frac{0.007}{0.595} \\ &= 0.012 \end{aligned} \quad (11)$$

4.1.4. Dempster–Shafer Decision Rule

After computing the mass functions, it is necessary to apply a decision rule to assign each pixel to one hypothesis of the DF. The usual decision rules related to the DST are threefold:

- **The maximum credibility** focuses on singletons only (i.e., it does not integrate uncertainty) and thus refers to a “pessimistic decision rule” (e.g., $credibility_{OP} = 0.664$ in Application 1).
- **The maximum plausibility** equals the sum of the credibility and uncertainty, thus referring to an “optimistic decision rule” (e.g., $plausibility_{OP} = 0.676$ in Application 1).
- **The maximum pignistic probability** equals the sum of the credibility and half of the uncertainty and thus refers to a “careful decision rule” (e.g., $pignisticprobability_{OP} = 0.67$ in Application 1).

That being said, dealing with high conflict values is a well-known limitation of DST that affects decision making [74] and has been regularly highlighted in previous studies [34,36–42]. To address this issue, we implemented a different decision rule that distributes the conflict by adapting the proportional conflict redistribution approach proposed by Smarandache and Dezert [75]. In concrete terms, the redistribution is based on the statistical validation of each hypothesis derived from the GAVEAU sample. Thus, the error matrices present more false positives (i.e., errors of commission) than false negatives (i.e., errors of omission), reflecting an underestimation of the OP class. We have therefore fully added the K_c conflict to the belief value of the OP hypothesis ($Belief_{OP}$). Finally, the decision making needed to define the DST fused class equals the maximum belief value, as in Equation (12).

$$DST_{class} = \begin{cases} OP, & \text{if } Belief_{OP} \geq Belief_{NOP} \\ NOP, & \text{otherwise} \end{cases} \quad (12)$$

4.2. Implementation of the Dempster–Shafer Theory

The DST was applied to different combinations of input sources to test the sensitivity of the fusion approach. For the sake of readability, these tests are hereafter called DST_{DIXM} , DST_{IXM} , DST_{DXM} , DST_{DIM} , DST_{DIX} , and DST_{Proba_D} , based on the first letter of the map’s name. DST_{DIXM} was computed with the four input maps. DST_{IXM} , DST_{DXM} , DST_{DIM} , and DST_{DIX} were computed with three input maps. Importantly, the DST_{Proba_D} test used the four input maps as for DST_{DIXM} , but the mass functions for DESCALS map were directly retrieved at pixel-level from a map of probabilities of pixels to belong to the OP class [59].

The DST then produces three output maps:

- **A belief map** of the OP hypothesis, i.e., a map of $Belief_{OP}$ values,
- **A conflict map**, i.e., a map of $1 - K_c$ values ranging from 0 (complete agreement between sources) to 1 (complete disagreement between sources),
- **A DST decision map** for the year 2019 with two classes, i.e., OP/NOP.

4.3. Validation Framework

In order to assess the accuracy of the DST decision map resulting from the fusion process, we proceeded in three steps.

Firstly, we computed a statistical validation based on the Kappa index. To do so, we relied on the GAVEAU test sample to evaluate DST improvement for OP map accuracy compared to the input sources. Then, to assess the spatial variability of the map’s accuracy at a finer scale, we mapped the Kappa index of the DST decision map for each tile defined during the sampling step (i.e., 723 tiles of 900 km² each).

Secondly, we analyzed if the spatial variability in Kappa values was related to the agricultural landscape composition (Figure 3). As a composition metric, we computed the ratio between the areas in smallholder and industrial plantations for each tile based on the GAVEAU reference map. Thus, metric values higher (lower) than 1 indicate the predominance of smallholder (industrial) plantations. We then conducted a statistical analysis, considering tiles with a significant OP area (larger than 5% of the tile's area). We applied the Kruskal–Wallis test to assess the Kappa index distribution for different landscape composition categories. This test focuses on population medians and proposes to test a null hypothesis H_0 (i.e., the distribution of the Kappa values is not significantly different for each category of landscape composition) at the 0.05 significance level. Then, the Compact Letter Display (CLD) method [76] identifies the categories with statistically significant different distributions by labeling them with letters.

Finally, we analyzed the distribution of belief and conflict values for different land-cover/use classes (first considering OP vs. NOP and then industrial vs. smallholder plantations) in order to assess the potential of these continuous values to discriminate OP plantations (Figure 3).

5. Results

The results are divided into statistical and spatial outputs through (1) MFA results, (2) the statistical validation of DST decision maps, and (3) a spatial variability assessment.

5.1. Mass Functions Assignment

The MFA for each hypothesis (OP, NOP, and union of hypotheses) is based on the statistical validation of each input source performed with the GAVEAU training sample (Table 2). The Kappa values ranged from 0.489 (XU map) to 0.724 (DESCALS map), illustrating the input sources' heterogeneity. We note that these values differed significantly from the validation values claimed by the authors in their publications (see Table 1). The heterogeneity of input sources also resulted in discrepancies in estimating OP areas in Sumatra (ranging from about 6.5 Mha for DESCALS, IIASA, and XU to more than 8 Mha for MAPBIOMAS). These statistical validations emphasized the importance of spatial resolution for accurate OP mapping since, as one might expect, the XU map at 100 m spatial resolution achieved less accurate results than the 10 m spatial-resolution DESCALS map.

Table 2. Kappa values and total OP areas for each input source.

Maps	Kappa with Training Sample	Kappa with Test Sample	OP Area (Ha)
DESCALS	0.724	0.725	6,821,655
IIASA	0.652	0.655	6,334,515
XU	0.489	0.493	6,835,993
MAPBIOMAS	0.643	0.649	8,174,029

Finally, since the mass functions assigned to the OP/NOP hypotheses for each input source were derived from the Kappa index, the highest and lowest mass functions were respectively computed for DESCALS and XU maps, whereas intermediate values were assigned to IIASA and MAPBIOMAS maps. These mass functions are introduced in Table 3 and must be interpreted as follows. Considering the DESCALS map as the input source, if a pixel was classified as OP, the masses for this pixel corresponding to OP or NOP hypothesis were $\theta_{OP|OP} = 0.724$ and $\theta_{NOP|OP} = 0.003$, respectively, with an associated uncertainty $\theta_{OP \cup NOP|OP} = 0.272$. Contrarily, if a pixel was classified as NOP in the DESCALS map, the masses for this pixel corresponding to NOP and OP were $\theta_{NOP|NOP} = 0.724$ and

$\theta_{OP}|\theta_{NOP} = 0.096$, respectively, with an associated uncertainty $\theta_{OPUNOP}|\theta_{NOP} = 0.178$. In this regard, the MFA stage assigned higher uncertainties for OP than for NOP for all input sources, since the OP class was poorly detected compared to the NOP class.

Table 3. Mass functions assigned for each input map.

Sources		θ_{OP}	θ_{NOP}	θ_{OPUNOP}
DESCALS	θ_{OP}	0.724	0.003	0.272
	θ_{NOP}	0.096	0.724	0.178
IIASA	θ_{OP}	0.652	0.005	0.342
	θ_{NOP}	0.147	0.652	0.200
XU	θ_{OP}	0.489	0.021	0.489
	θ_{NOP}	0.268	0.489	0.242
MAPBIOMAS	θ_{OP}	0.642	0.013	0.344
	θ_{NOP}	0.128	0.642	0.229

5.2. Statistical Validation of the DST Decision Map

Once mass functions were assigned to each hypothesis, we applied the DST to all combinations of input sources defined in Section 4.2. The resulting maps were then statistically validated with the GAVEAU test sample (Table 4). The major results to be emphasized are threefold.

Table 4. Statistical validation indices (Kappa) and OP area estimates for each fusion test.

Fused Map	Kappa	OP Area (Ha)
DST_{DIXM}	0.749	7,504,349
DST_{IXM}	0.709	9,967,305
DST_{DXM}	0.740	10,114,982
DST_{DIM}	0.740	10,114,982
DST_{DIX}	0.756	8,071,561
DST_{Proba_D}	0.780	8,310,400

First, for most of the combinations, the Kappa values of the DST decision maps were higher than the Kappa value of the most accurate input source. The lowest Kappa value (i.e., $Kappa = 0.709$) was achieved by the DST_{IXM} test, which was the only combination not to consider the DESCALS map (the most valued map at MFA).

Second, integrating more input sources did not necessarily improve the results. For example, the DST_{DIX} 3-sources combination achieved higher results than the DST_{DIXM} combination. Adding sources carried conflicting information, thus increasing uncertainty and penalizing the final results. Moreover, DST_{DIM} and DST_{DXM} presented similar results, highlighting that the input sources may sometimes not provide original information.

Third, the integration of pixel-level probability provided by the map producers (i.e., probabilities associated with the DESCALS map) increased the results achieving the highest Kappa value (i.e., $Kappa = 0.780$) for DST_{Proba_D} , higher than the best Kappa value for a single input source (Kappa of DESCALS map = 0.724).

In addition, the resulting OP areas for Sumatra ranged from 7.5 Mha (DST_{DIXM}) to 10.1 Mha (DST_{DIM} and DST_{DXM}) and confirmed the quality of the DST_{Proba_D} map, whose OP area (8,310,400 Ha) was close to the 2019 OP area estimated by the Indonesian Ministry of Agriculture (8,299,729 Ha) for Sumatra [77]. For these reasons, the DST_{Proba_D} map was considered for further analysis.

Kappa values at the tile scale (between 0.6 and 0.8 for 30% of tiles) reflected the results achieved at the Sumatra scale but also revealed (1) extreme values (Kappa < 0.2 for 3% of tiles and >0.8 for 10% of tiles) and (2) strong spatial heterogeneity (Figure 6). Interestingly, the spatial distribution of Kappa values did not follow any spatial trend (neither the north–south nor east–west gradient), and was instead explained by (1) tiles with unbalanced reference points between OP/NOP, as low Kappa values were often observed in tiles at the interfaces with NOP; (2) tiles with large classification errors, as observed in southern Riau province (see Figure 6) where low Kappa values corresponded to coconut plantations confused with OP plantations [78]; and (3) the predominance of a plantation type (high Kappa values characterize a predominance of industrial plantations).

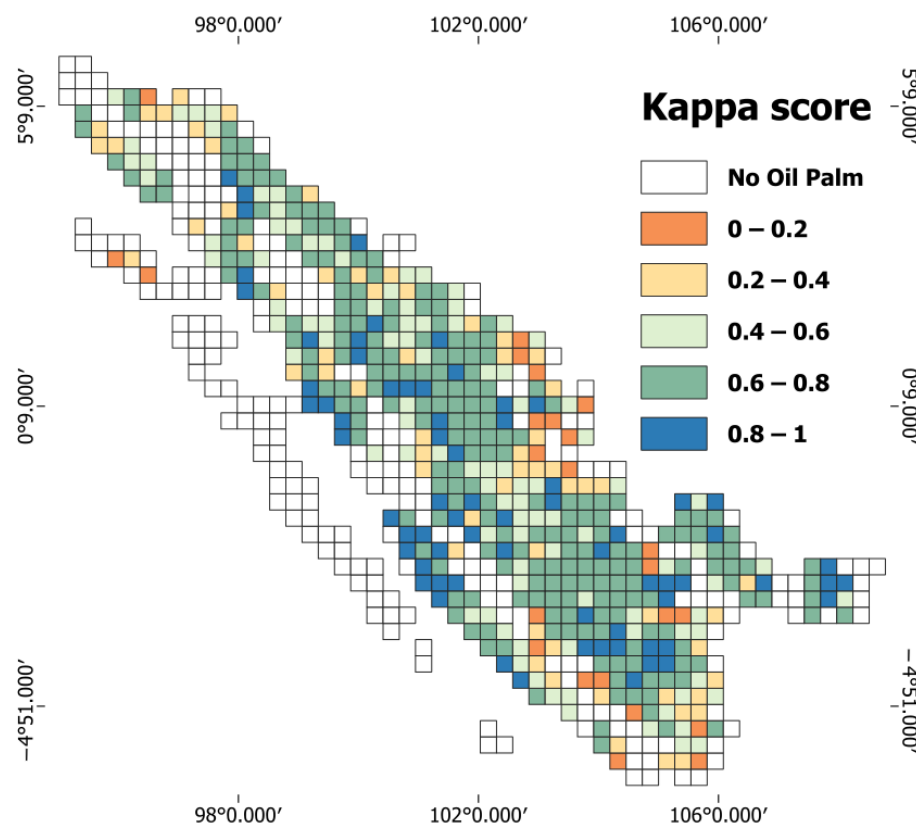


Figure 6. The distribution of Kappa values at the tile scale for the DST_{Proba_D} fused map.

5.3. Spatial Variability Assessment

Beyond the binary DST decision map, the DST also provided more continuous information through (1) the belief map for the OP hypothesis and (2) the conflict map between input sources (Figure 7).

Hence, the belief map for the OP hypothesis highlighted that 87% of Sumatra's area was characterized by very low (≤ 0.2) or high (≥ 0.8) belief values (Figure 7). In that case, low belief values corresponded to high certainty for NOP areas, and high belief values corresponded to high certainty for OP areas. In order to illustrate this variability, Figure 7B shows that higher belief values were observed in tiles with homogeneous landscapes dominated by industrial plantations, whereas low belief values were encountered in fragmented landscapes with a predominance of smallholder plantations (Figure 7C). These findings were confirmed by Figure 8B, which shows different distributions of belief values for the reference points of smallholder (lower belief values) and industrial plantations (higher belief values).

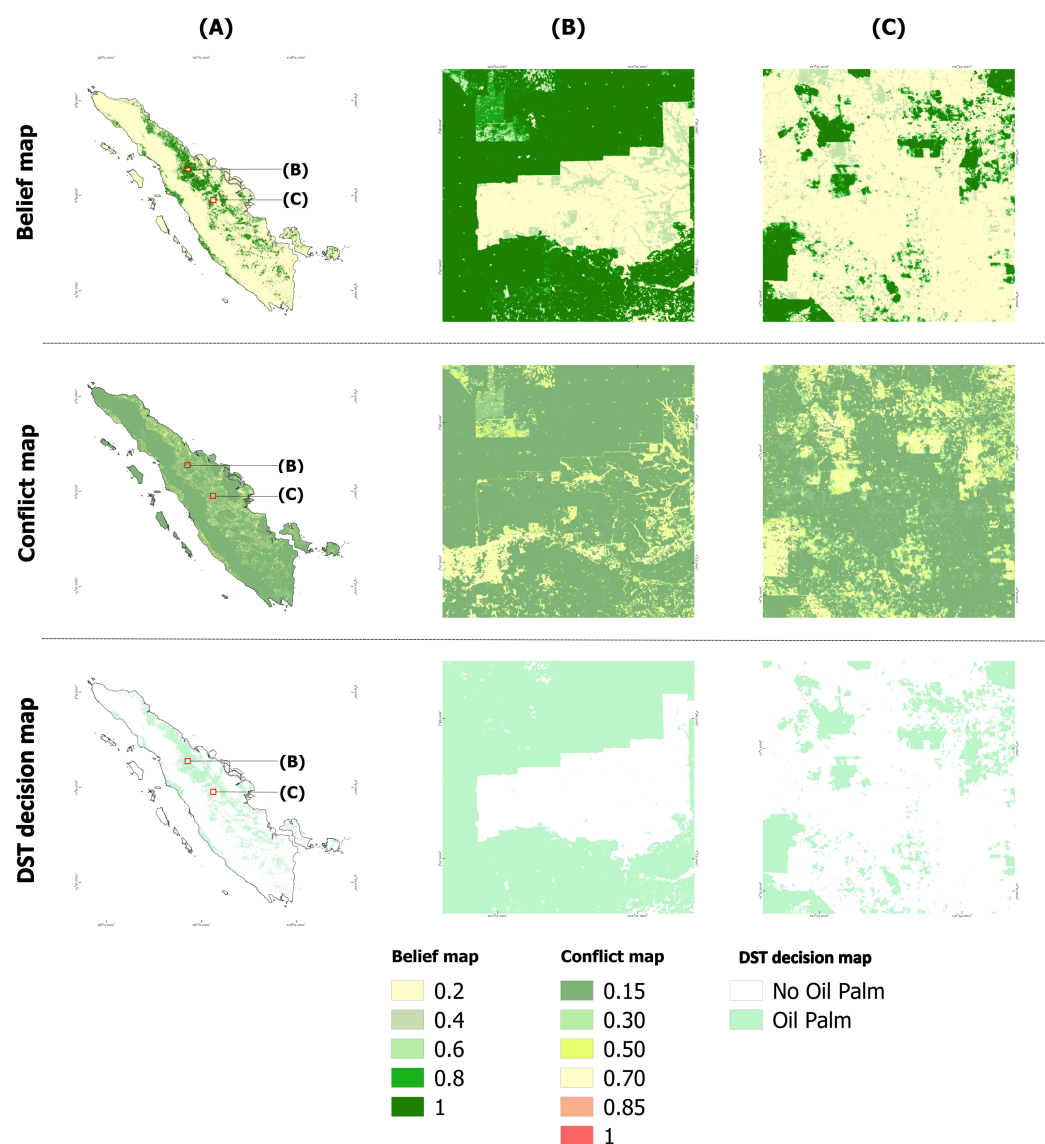


Figure 7. Belief, conflict, and DST decision maps resulting from the application of the Dempster–Shafer theory at (A) the Sumatra scale and for two tiles characterized by the predominance of (B) industrial OP plantations and (C) smallholder OP plantations.

In contrast, 89% of Sumatra’s area was characterized by low conflict values ($K_c < 0.3$), reflecting a global agreement between the input sources (Figure 7). However, medium to high conflict values ($K_c > 0.5$) were mainly located in areas considered OP, highlighting the challenge of OP detection. This was confirmed by the distribution of conflict values for reference points, since points belonging to the OP class showed higher conflict values than points of the NOP class (Figure 8A). Moreover, a tile-level analysis showed significant spatial variability, with OP areas predominated by industrial plantations (Figure 7B) presenting lower conflict values than OP areas predominated by smallholder plantations (Figure 7C). Figure 8A also emphasizes that the disagreement between input sources was higher for smallholder than for industrial plantations.

Finally, the metric of landscape composition comparing the areas of smallholder and industrial plantations for each tile showed a decrease in median Kappa values, as smallholder plantations became larger than industrial plantations (Figure 9). The distribution of Kappa values was only significantly different for tiles where the area of smallholder plantations was two times greater than the area of industrial plantations (Figure 9).

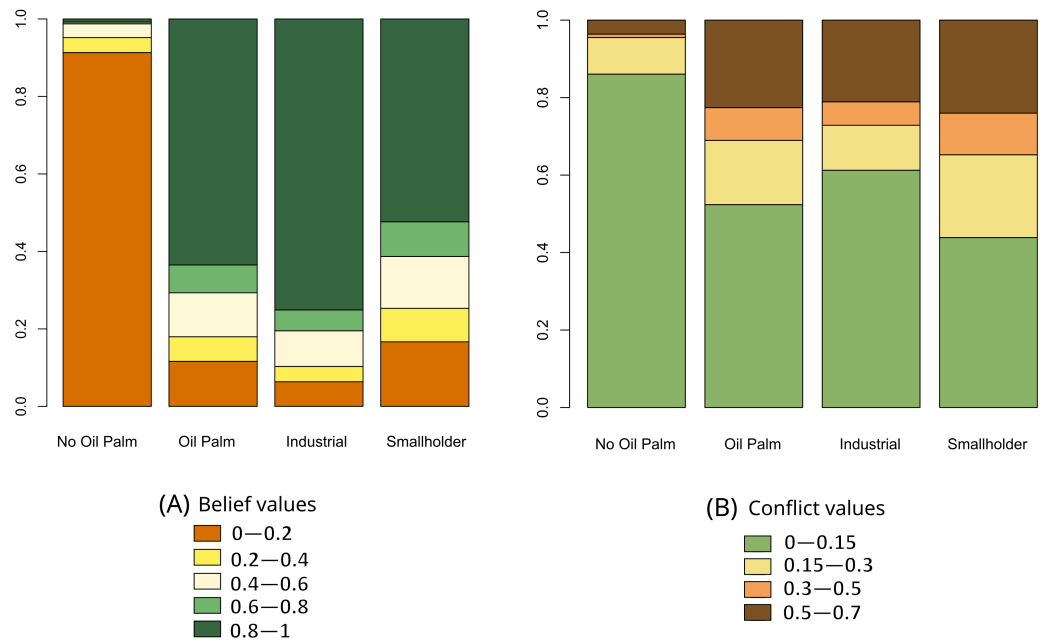


Figure 8. Distribution of reference points according to their land-use class for (A) values of belief between input sources and (B) values of conflict in each hypothesis

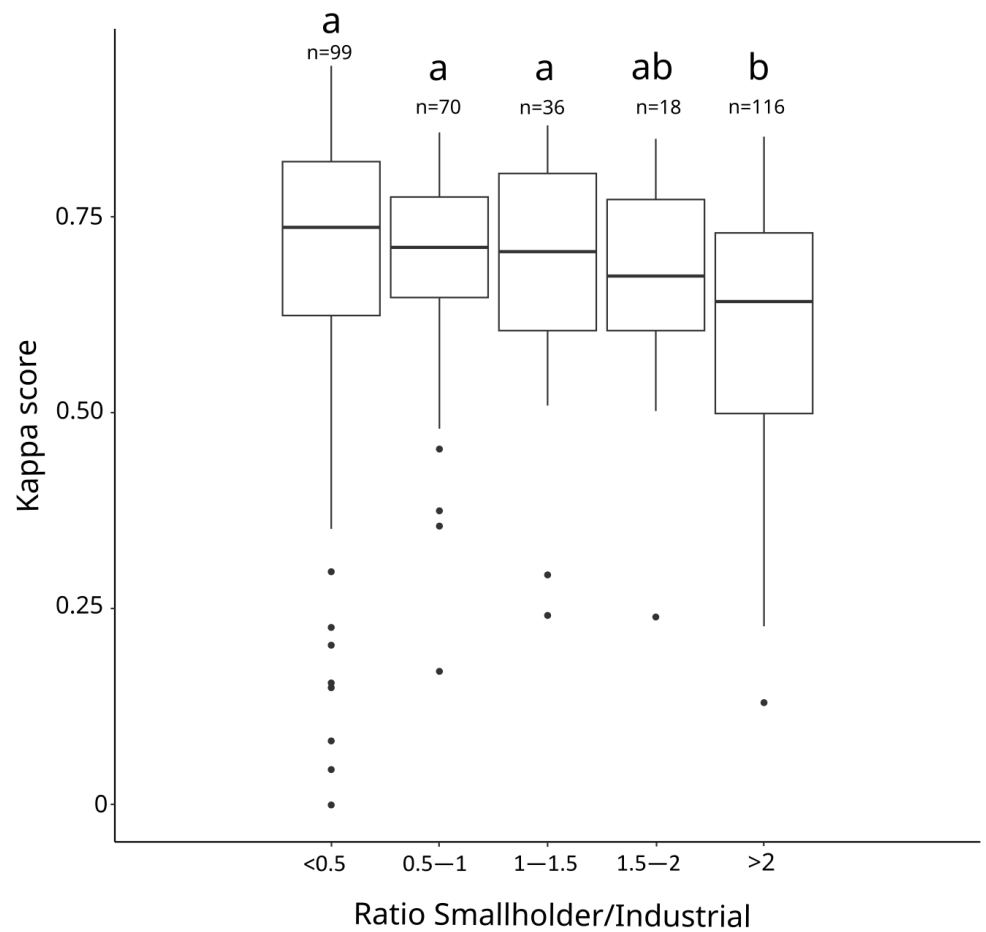


Figure 9. The distribution of Kappa values according to the landscape composition metric (i.e., ratio between smallholder and industrial plantations) at tile-scale. Letters *a* and *b* produced by CLD method indicate statistically significant different distributions.

6. Discussion

We produced a map of OP plantations at Sumatra-scale by combining four heterogeneous maps using the Dempster–Shafer theory. Our results showed that applying the DST significantly improved the classification accuracy (Kappa = 0.78 vs. best Kappa of input sources = 0.724) and allowed for quantifying and mapping (1) belief values in the detection of OP plantations and (2) conflict values between input sources. The results also highlighted the methodological challenge of detecting OP plantations, especially smallholder plantations [44,59,61,62]. However, although promising, our results raise numerous methodological issues that must be discussed.

The first issue refers to the definition of the discernment framework. At this stage, all input maps must share common characteristics. Here, we resampled all maps at 10 m spatial resolution with a nearest-neighbor approach. However, complementary tests at a moderate resolution (e.g., 30 or 100 m) may be relevant, since a coarser resolution may reduce uncertainties, although generating less spatially detailed results. Also, other resampling approaches may be tested to derive pixel-level probabilities to be further integrated in the fusion process. Moreover, while we limited our application to OP and NOP classes, more tests would be relevant to assess the potential of DST to discriminate finer classes. Moreover, setting the hypotheses emphasized an important issue regarding potential discrepancies between definitions of OP plantations in the different input sources. For example, the OP class in the DESCALS map corresponded to closed mature canopy plantations, whereas other input sources might have also integrated young or failed plantations (e.g., GAVEAU).

In addition, discrepancies in OP definitions between two input sources or between an input source and the GAVEAU reference map may also impact the MFA stage. Indeed, such discrepancies may penalize the statistical validation of the input source that used a definition different from the reference map, consequently leading to low estimates of mass functions. This point may explain the differences between the validation results claimed by the map producers and our validation results. However, these differences may also be due to different validation approaches (e.g., stratified sampling vs. regular or random sampling) and different reference samples (e.g., including samples in smallholder plantations or not, or considering only mature plantations, or integrating young plantations).

Still considering the MFA stage, the statistical validation of input sources here relied on a single statistical index and a single reference sample (i.e., GAVEAU training sample). We here considered the Kappa index, but other accuracy indices (e.g., F1-score or user and producer accuracies, [71]) may also be tested to determine the mass functions for each hypothesis. Overall, this point also questions the application of our approach when no reference map is available. For this reason, it is essential (1) that map producers harmonize the validation procedures to ensure that accuracy metrics can be compared and reused in data fusion process and (2) to implement unsupervised strategies to assign mass functions, e.g., by assessing cross-agreement levels between input sources in order to identify the most- and least-reliable maps. More importantly, our best result was achieved by including the map of probabilities provided by DESCALS, emphasizing the relevance of considering mass functions at a pixel level (instead of a class level, as done for other tests). Consequently, we recommend map producers to release the intermediate probability maps and not only the final classifications. Meanwhile, attempts to estimate mass functions at the pixel level considering ancillary information (e.g., landscape metrics, number of observations in time series, distance to patch edges) may also be relevant.

Regarding the DST fusion rule, the main issue refers to the conflict redistribution rule. In the present case, we distributed the conflict entirely over the OP class to compensate for the fact that mass functions assigned to the OP class were lower than those assigned to

the NOP class (i.e., $\theta_{OP}|\theta_{NOP} < \theta_{NOP}|\theta_{OP}$ in Figure 5 and Table 3). However, considering additional land-cover classes (industrial and smallholder plantations) would require the use of different methods for conflict distribution (e.g., the proportional conflict redistribution rule [75]).

In addition, the decision rule based on the maximum belief value between the OP and NOP hypotheses (see Equation (12)) may be discussed for the specific case of binary classifications, as in the present study. Indeed, since most input sources poorly detected smallholder plantations, many of these plantations were characterized by low $Belief_{OP}$ values, so it may be relevant to lower the OP detection threshold in order to capture more OP areas. By considering different decision rules, it would also be possible to derive different OP maps corresponding to different definitions of OP plantations, as also proposed in Arvor et al. [79]. For example, a restrictive map may only focus on pixels with high $Belief_{OP}$ values, whereas a broad map may consider pixels with moderate to high $Belief_{OP}$ values. Such maps may carry relevant information for end-users from various scientific domains (e.g., ecologists computing landscape metrics or economists dealing with administrative-level uncertainties).

At the validation stage, we have shown that the spatial variability of Kappa values was related to the proportion of industrial and smallholder OP plantations in tiles. This metric of landscape composition only provides a partial description of the local landscape, so additional metrics of landscape configuration (e.g., aggregation index, cohesion [80]), number of patches) should be tested in order to better assess the impact of landscape structure on the potential to map OP plantations, especially considering different plantation types (smallholder vs. industrial plantations).

Finally, this work highlights the strengths of DST, particularly in its management of uncertainty and ignorance. However, other data fusion methods (e.g., fuzzy logics, voting strategies; see Section 1) should be tested and compared in order to highlight the strengths and limitations of each approach for OP mapping. In this regard, we added a comparison with voting strategy data fusion in the Appendix A.

7. Conclusions

The multiplication of remote sensing-based land-cover/use maps through the continuous development of remote sensors and computing capabilities is opening up promising prospects while raising essential issues. Especially, it questions the potential of such a proliferation of information to effectively support the implementation and monitoring of important land-use policies (e.g., EUDR), rather than somehow confusing end-users looking for the most appropriate data to meet their specific needs. In this context, we assessed the potential of the Dempster–Shafer theory to combine independent and heterogeneous large-scale land-cover maps at a moderate (30 m) pixel resolution. The operational application of DST relied on the automatic setting of mass functions (although requiring a reference source) and the improved distribution of conflict between hypotheses. Our results showed that the Dempster–Shafer theory was efficient in combining four maps of oil palm plantations in Sumatra island, taking advantage of the strengths of each product. Despite the shortcomings of the input maps related to the specific application considered in this study (i.e., different OP definitions and probability map only available for one input source), the DST produced a significantly more accurate fused map of OP plantations. Beyond the discrete binary OP/NOP maps, belief and conflict maps also presented interesting continuous information, whose potential to better categorize OP plantations and assess the OP dynamics and consequent socio-environmental impacts needs to be explored.

Author Contributions: The concept for this work was developed by C.B., S.C., D.A. and J.G. during discussions within the ANR PALMEXPAND project. The methodology was implemented by C.B., D.A., T.C. and S.C., and the software application was developed by C.B., T.C. and D.A. All data and resources used were collected by C.B. with the participation of A.D., D.G., J.H. and C.C.-B. for validation data. All authors participated in the drafting and proofreading of the original draft, and C.B. and D.A. modified and revised the revised draft. Visualization was carried out by C.B. Project supervision was led by D.A., S.C. and J.G. Finally, J.G., S.C. and D.A. managed the administration and acquisition of project funds. All authors have read and approved the published version of the manuscript.

Funding: This work was supported by the Région Bretagne (France), the French National Research Agency (ANR) through the Palmexpand project (grant agreement: ANR-20-CE03-0004) and the French National Centre for Space Studies (CNES) through the SEMTI-SENT project (grant agreement 274217). Jérémie Gignoux and Julia Hélie thank the support of the EUR grant ANR-17-EURE-0001. Julia Hélie also thanks the support of INRAE and CIRAD UMR ABSys.

Data Availability Statement: All data and codes used are available on a GitHub directory: <https://github.com/CarlBethuel/Dempster-Shafer-work>, accessed on 8 January 2025.

Conflicts of Interest: Author David Gaveau was employed by the company TheTreeMap. The remaining authors declare that the research was conducted in the absence of any commercial or financial relationships that could be construed as a potential conflict of interest.

Appendix A. Data Fusion with Voting Strategies

In order to compare the DST results with another fusion method, we also tested a voting strategy fusion. This approach aggregates predictions from multiple sources using voting systems (e.g., simple majority voting or weighted voting), i.e., a vote assigned to each input map. There are several examples of applications of this approach, such as the “convergence of evidence” method in the Whisp platform. Also, Shen et al. [81] or Wang et al. [82] applied voting strategies to classify land-cover using remote sensing data. Although the voting strategy approach is easy to implement, uncertainty management remains limited. However, this is an essential point in our work, since the diversity of oil palm plantation maps and the methodological challenges involved in these mappings induce significant uncertainties in the results. Whereas our paper therefore focuses on the application of DST, we also tested the voting strategy approach using weights. In that case, each weight is assigned to pixels depending on their class, OP or NOP. Then, if the sum of all votes is greater than or equal to 0.5, we consider the pixel to correspond as OP; otherwise, we classify it as NOP.

We tested this approach with two types of weights : (1) all weights equally set to 1, and (2) all weights set depending on Kappa index associated to each input map..

The results showed high Kappa index values ($K_p = 0.749$ for equal weights and $K_p = 0.725$ for Kappa weights), but these still lower than those obtained by applying the DST method ($K_p = 0.780$). Thus, we can conclude that (1) the results were comparable to those obtained with DST (K_p for $DST_{DIX} = 0.756$) without considering probability maps and (2) it emphasizes the importance of considering probability maps to improve the fusion results (K_p for $DST_{Proba_D} = 0.780$). It is also important to note that voting-based methods do not spatialize conflict between sources or manage uncertainty, which are key aspects in improving the reliability of fusion outcomes. Thus, we can conclude that (1) the results were comparable to those obtained with DST (K_p for $DST_{DIX} = 0.756$) without considering probability maps, and (2) it emphasizes the importance of considering probability maps to improve the fusion results (K_p for $DST_{Proba_D} = 0.780$).

References

1. Gorelick, N.; Hancher, M.; Dixon, M.; Ilyushchenko, S.; Thau, D.; Moore, R. Google Earth Engine: Planetary-scale geospatial analysis for everyone. *Remote Sens. Environ.* **2017**, *202*, 18–27. [[CrossRef](#)]
2. Mahecha, M.D.; Gans, F.; Brandt, G.; Christiansen, R.; Cornell, S.E.; Fomferra, N.; Kraemer, G.; Peters, J.; Bodesheim, P.; Camps-Valls, G.; et al. Earth system data cubes unravel global multivariate dynamics. *Earth Syst. Dyn.* **2020**, *11*, 201–234. [[CrossRef](#)]
3. Congalton, R.G.; Gu, J.; Yadav, K.; Thenkabail, P.; Ozdogan, M. Global Land Cover Mapping: A Review and Uncertainty Analysis. *Remote Sens.* **2014**, *6*, 12070–12093. [[CrossRef](#)]
4. Grekousis, G.; Mountrakis, G.; Kavouras, M. An overview of 21 global and 43 regional land-cover mapping products. *Int. J. Remote Sens.* **2015**, *36*, 5309–5335. [[CrossRef](#)]
5. Hansen, M.C.; Potapov, P.V.; Moore, R.; Hancher, M.; Turubanova, S.A.; Tyukavina, A.; Thau, D.; Stehman, S.V.; Goetz, S.J.; Loveland, T.R.; et al. High-Resolution Global Maps of 21st-Century Forest Cover Change. *Science* **2013**, *342*, 850–853. [[CrossRef](#)]
6. Vancutsem, C.; Achard, F.; Pekel, J.F.; Vieilledent, G.; Carboni, S.; Simonetti, D.; Gallego, J.; Aragão, L.E.O.C.; Nasi, R. Long-term (1990–2019) monitoring of forest cover changes in the humid tropics. *Sci. Adv.* **2021**, *7*, eabe1603. [[CrossRef](#)] [[PubMed](#)]
7. Pekel, J.F.; Cottam, A.; Gorelick, N.; Belward, A.S. High-resolution mapping of global surface water and its long-term changes. *Nature* **2016**, *540*, 418–422. [[CrossRef](#)] [[PubMed](#)]
8. Ximenes, A.C.; Cavanaugh, K.C.; Arvor, D.; Murdiyarso, D.; Thomas, N.; Arcoverde, G.F.B.; Bispo, P.d.C.; Van der Stocken, T. A comparison of global mangrove maps: Assessing spatial and bioclimatic discrepancies at poleward range limits. *Sci. Total Environ.* **2023**, *860*, 160380. [[CrossRef](#)]
9. Venter, Z.S.; Barton, D.N.; Chakraborty, T.; Simensen, T.; Singh, G. Global 10 m Land Use Land Cover Datasets: A Comparison of Dynamic World, World Cover and Esri Land Cover. *Remote Sens.* **2022**, *14*, 4101. [[CrossRef](#)]
10. Inglada, J.; Vincent, A.; Arias, M.; Tardy, B. iota2 Chain, 2016. Available online: <https://zenodo.org/records/58150> (accessed on 8 January 2025).
11. Souza, C.; Shimbo, J.; Rosa, M.; Parente, L.; Alencar, A.; Rudorff, B.; Hasenack, H.; Matsumoto, M.; Ferreira, L.; Souza-Filho, P.W.M.; et al. Reconstructing Three Decades of Land Use and Land Cover Changes in Brazilian Biomes with Landsat Archive and Earth Engine. *Remote Sens.* **2020**, *12*, 2735. [[CrossRef](#)]
12. Oliphant, A.J.; Thenkabail, P.S.; Teluguntla, P.; Xiong, J.; Gumma, M.K.; Congalton, R.G.; Yadav, K. Mapping cropland extent of Southeast and Northeast Asia using multi-year time-series Landsat 30-m data using a random forest classifier on the Google Earth Engine Cloud. *Int. J. Appl. Earth Obs. Geoinf.* **2019**, *81*, 110–124. [[CrossRef](#)]
13. Broich, M.; Hansen, M.C.; Potapov, P.; Adusei, B.; Lindquist, E.; Stehman, S.V. Time-series analysis of multi-resolution optical imagery for quantifying forest cover loss in Sumatra and Kalimantan, Indonesia. *Int. J. Appl. Earth Obs. Geoinf.* **2011**, *13*, 277–291. [[CrossRef](#)]
14. Xiao, H.; Su, F.; Fu, D.; Lyne, V.; Liu, G.; Pan, T.; Teng, J. Optimal and robust vegetation mapping in complex environments using multiple satellite imagery: Application to mangroves in Southeast Asia. *Int. J. Appl. Earth Obs. Geoinf.* **2021**, *99*, 102320. [[CrossRef](#)]
15. Xiao, C.; Li, P.; Feng, Z. Monitoring annual dynamics of mature rubber plantations in Xishuangbanna during 1987–2018 using Landsat time series data: A multiple normalization approach. *Int. J. Appl. Earth Obs. Geoinf.* **2019**, *77*, 30–41. [[CrossRef](#)]
16. Zhang, C.; Xiao, X.; Zhao, L.; Qin, Y.; Doughty, R.; Wang, X.; Dong, J.; Yang, X. Mapping Eucalyptus plantation in Guangxi, China by using knowledge-based algorithms and PALSAR-2, Sentinel-2, and Landsat images in 2020. *Int. J. Appl. Earth Obs. Geoinf.* **2023**, *120*, 103348. [[CrossRef](#)]
17. Gilbert, C.L. The EU Deforestation Regulation. *EuroChoices* **2024**, *23*, 64–70. [[CrossRef](#)]
18. D’Annunzio, R.; O’Brien, V.; Arnell, A.; Neeff, T.; Fontanarosa, R.; Valbuena Perez, P.; Shapiro, A.C.; Sanchez-Paus Diaz, A.; Merle, C.; Vega, J.; et al. *Towards a Digital Public Infrastructure for Deforestation-Related Trade Regulations*; FAO: Rome, Italy, 2024.
19. Bloch, I.; Maître, H. Fusion de données en traitement d’images: Modèles d’information et décisions. *Trait. Du Signal* **1994**, *11*, 435–446.
20. Dasarathy, B. Sensor fusion potential exploitation-innovative architectures and illustrative applications. *Proc. IEEE* **1997**, *85*, 24–38. [[CrossRef](#)]
21. Benediktsson, J.; Sveinsson, J. Classification of hyperdimensional data using data fusion approaches. In Proceedings of the IGARSS’97, 1997 IEEE International Geoscience and Remote Sensing Symposium Proceedings, Remote Sensing—A Scientific Vision for Sustainable Development, Singapore, 3–8 August 1997; Volume 4, pp. 1669–1671. [[CrossRef](#)]
22. Zhang, J. Multi-source remote sensing data fusion: Status and trends. *Int. J. Image Data Fusion* **2010**, *1*, 5–24. [[CrossRef](#)]
23. Belgiu, M.; Stein, A. Spatiotemporal Image Fusion in Remote Sensing. *Remote Sens.* **2019**, *11*, 818. [[CrossRef](#)]
24. Castanedo, F. A Review of Data Fusion Techniques. *Sci. World J.* **2013**, *2013*, 704504. [[CrossRef](#)] [[PubMed](#)]
25. Schmitt, M.; Zhu, X.X. Data Fusion and Remote Sensing: An ever-growing relationship. *IEEE Geosci. Remote Sens. Mag.* **2016**, *4*, 6–23. [[CrossRef](#)]

26. Dogan, A.; Birant, D. A Weighted Majority Voting Ensemble Approach for Classification. In Proceedings of the 2019 4th International Conference on Computer Science and Engineering (UBMK), Samsun, Turkey, 11–15 September 2019; pp. 1–6. [[CrossRef](#)]
27. Fauvel, M.; Chanussot, J.; Benediktsson, J. Decision Fusion for the Classification of Urban Remote Sensing Images. *IEEE Trans. Geosci. Remote Sens.* **2006**, *44*, 2828–2838. [[CrossRef](#)]
28. Murmu, S.; Biswas, S. Application of Fuzzy Logic and Neural Network in Crop Classification: A Review. *Aquat. Procedia* **2015**, *4*, 1203–1210. [[CrossRef](#)]
29. Zadeh, L.A. Fuzzy sets. *Inf. Control* **1965**, *8*, 338–353. [[CrossRef](#)]
30. Zeng, Y.; Zhang, J.; Genderen, J.L.v. Comparison and analysis of remote sensing data fusion techniques at feature and decision levels. In Proceedings of the ISPRS Commission VII Symposium: Remote Sensing: From Pixels to Processes, Enschede, The Netherlands, 8–11 May 2006; International Institute for Geo-Information Science and Earth Observation: Enschede, The Netherlands, 2006.
31. Shoshany, M.; Cohen, Y. Inference versus evidence in reasoning remote sensing recognition, with an information foraging perspective. *Int. J. Remote Sens.* **2007**, *28*, 2613–2634. [[CrossRef](#)]
32. Dempster, A.P. Upper and Lower Probabilities Induced by a Multivalued Mapping. *Ann. Math. Stat.* **1967**, *38*, 325–339. [[CrossRef](#)]
33. Shafer, G. *A Mathematical Theory of Evidence*; Princeton Univ. Press: Princeton, NJ, USA, 1976.
34. Lein, J.K. Applying evidential reasoning methods to agricultural land cover classification. *Int. J. Remote Sens.* **2003**, *24*, 4161–4180. [[CrossRef](#)]
35. Wang, J.; Qiao, K.; Zhang, Z.; Xiang, F. A new conflict management method in Dempster–Shafer theory. *Int. J. Distrib. Sens. Netw.* **2017**, *13*, 1550147717696506. [[CrossRef](#)]
36. Le Hegarat-Masclé, S.; Bloch, I.; Vidal-Madjar, D. Application of Dempster-Shafer evidence theory to unsupervised classification in multisource remote sensing. *IEEE Trans. Geosci. Remote Sens.* **1997**, *35*, 1018–1031. [[CrossRef](#)]
37. Ran, Y.; Li, X.; Lu, L.; Li, Z. Large-scale land cover mapping with the integration of multi-source information based on the Dempster–Shafer theory. *Int. J. Geogr. Inf. Sci.* **2012**, *26*, 169–191. [[CrossRef](#)]
38. Hao, S.; Chen, Y.; Hu, B.; Cui, Y. A classifier-combined method based on D-S evidence theory for the land cover classification of the Tibetan Plateau. *Environ. Sci. Pollut. Res.* **2021**, *28*, 16152–16164. [[CrossRef](#)] [[PubMed](#)]
39. Cayuela, L.; Golicher, J.D.; Rey, J.S.; Benayas, J.M.R. Classification of a complex landscape using Dempster–Shafer theory of evidence. *Int. J. Remote Sens.* **2006**, *27*, 1951–1971. [[CrossRef](#)]
40. Mora, B.; Fournier, R.A.; Foucher, S. Application of evidential reasoning to improve the mapping of regenerating forest stands. *Int. J. Appl. Earth Obs. Geoinf.* **2011**, *13*, 458–467. [[CrossRef](#)]
41. Yang, F.; Wei, H.; Feng, P. A hierarchical Dempster-Shafer evidence combination framework for urban area land cover classification. *Measurement* **2020**, *151*, 105916. [[CrossRef](#)]
42. Belmahdi, F.; Lazri, M.; Ouallouche, F.; Labadi, K.; Absi, R.; Ameer, S. Application of Dempster-Shafer theory for optimization of precipitation classification and estimation results from remote sensing data using machine learning. *Remote Sens. Appl. Soc. Environ.* **2023**, *29*, 100906. [[CrossRef](#)]
43. FAO. FAOSTAT Online Database. 2022. Available online: <http://faostat.fao.org> (accessed on 11 November 2022).
44. Gaveau, D.L.A.; Locatelli, B.; Salim, M.A.; Husnayaen; Manurung, T.; Descals, A.; Angelsen, A.; Meijaard, E.; Sheil, D. Slowing deforestation in Indonesia follows declining oil palm expansion and lower oil prices. *PLoS ONE* **2022**, *17*, e0266178. [[CrossRef](#)] [[PubMed](#)]
45. Widayatmoko, B.; Dewi, R. Dynamics of Transmigration Policy as Supporting Policy of Palm Oil Plantation Development in Indonesia. *J. Indones. Soc. Sci. Humanit.* **2019**, *9*, 35–55. [[CrossRef](#)]
46. Cramb, R.; McCarthy, J.F. *The Oil Palm Complex: Smallholders, Agribusiness and the State in Indonesia and Malaysia*; NUS Press: Singapore, 2016. [[CrossRef](#)]
47. Carlson, K.M.; Curran, L.M.; Asner, G.P.; Pittman, A.M.; Trigg, S.N.; Marion Adeney, J. Carbon emissions from forest conversion by Kalimantan oil palm plantations. *Nat. Clim. Change* **2013**, *3*, 283–287. [[CrossRef](#)]
48. Wilcove, D.S.; Koh, L.P. Addressing the threats to biodiversity from oil-palm agriculture. *Biodivers. Conserv.* **2010**, *19*, 999–1007. [[CrossRef](#)]
49. Comte, I.; Colin, F.; Whalen, J.K.; Grünberger, O.; Caliman, J.P. Chapter three—Agricultural Practices in Oil Palm Plantations and Their Impact on Hydrological Changes, Nutrient Fluxes and Water Quality in Indonesia: A Review. In *Advances in Agronomy*; Sparks, D.L., Ed.; Academic Press: New York, NY, USA, 2012; Volume 116, pp. 71–124. [[CrossRef](#)]
50. Colchester, M. *Palm Oil and Indigenous Peoples in South East Asia Land Acquisition, Human Rights Violations and Indigenous Peoples on the Palm Oil Frontier*; Technical Report; IUCN: Washington, DC, USA, 2010.
51. Qaim, M.; Sibhatu, K.T.; Siregar, H.; Grass, I. Environmental, Economic, and Social Consequences of the Oil Palm Boom. *Annu. Rev. Resour. Econ.* **2020**, *12*, 321–344. [[CrossRef](#)]

52. Chong, K.L.; Kanniah, K.D.; Pohl, C.; Tan, K.P. A review of remote sensing applications for oil palm studies. *Geo-Spat. Inf. Sci.* **2017**, *20*, 184–200. [[CrossRef](#)]
53. De Petris, S.; Boccardo, P.; Borgogno-Mondino, E. Detection and characterization of oil palm plantations through MODIS EVI time series. *Int. J. Remote Sens.* **2019**, *40*, 7297–7311. [[CrossRef](#)]
54. Oon, A.; Mohd Shafri, H.Z.; Lechner, A.M.; Azhar, B. Discriminating between large-scale oil palm plantations and smallholdings on tropical peatlands using vegetation indices and supervised classification of LANDSAT-8. *Int. J. Remote Sens.* **2019**, *40*, 7312–7328. [[CrossRef](#)]
55. Ramdani, F. Analysing variety of vegetation indices values using different methods for mapping oil palm closed-canopy composition in southern Riau Province, Indonesia. In Proceedings of the 2012 IEEE International Geoscience and Remote Sensing Symposium, Munich, Germany, 22–27 July 2012; pp. 6032–6034. [[CrossRef](#)]
56. Tridawati, A.; Darmawan, S.; Armijon. Estimation the oil palm age based on optical remote sensing image in Landak Regency, West Kalimantan Indonesia. *IOP Conf. Ser. Earth Environ. Sci.* **2018**, *169*, 012063. [[CrossRef](#)]
57. Xu, Y.; Yu, L.; Li, W.; Ciaia, P.; Cheng, Y.; Gong, P. Annual oil palm plantation maps in Malaysia and Indonesia from 2001 to 2016. *Earth Syst. Sci. Data* **2020**, *12*, 847–867. [[CrossRef](#)]
58. Descals, A.; Szantoi, Z.; Meijaard, E.; Sutikno, H.; Rindanata, G.; Wich, S. Oil Palm (*Elaeis guineensis*) Mapping with Details: Smallholder versus Industrial Plantations and their Extent in Riau, Sumatra. *Remote Sens.* **2019**, *11*, 2590. [[CrossRef](#)]
59. Descals, A.; Wich, S.; Meijaard, E.; Gaveau, D.L.A.; Peedell, S.; Szantoi, Z. High-resolution global map of smallholder and industrial closed-canopy oil palm plantations. *Earth Syst. Sci. Data* **2021**, *13*, 1211–1231. [[CrossRef](#)]
60. Cheng, Y.; Yu, L.; Xu, Y.; Lu, H.; Cracknell, A.P.; Kanniah, K.; Gong, P. Mapping oil palm extent in Malaysia using ALOS-2 PALSAR-2 data. *Int. J. Remote Sens.* **2018**, *39*, 432–452. [[CrossRef](#)]
61. Okarda, B.; Carolita, I.; Kartika, T.; Komarudin, H. Mapping of smallholder oil palm plantation and development of a growth model. *IOP Conf. Ser. Earth Environ. Sci.* **2018**, *169*, 012074. [[CrossRef](#)]
62. Yayusman, L.F.; Nagasawa, R. ALOS-Sensor data integration for the detection of smallholder's oil palm plantation in Southern Sumatra, Indonesia. *J. Jpn. Agric. Syst. Soc.* **2015**, *31*, 27–40. [[CrossRef](#)]
63. Ramdani, F. Recent expansion of oil palm plantation in the most eastern part of Indonesia: Feature extraction with polarimetric SAR. *Int. J. Remote Sens.* **2019**, *40*, 7371–7388. [[CrossRef](#)]
64. Oon, A.; Ngo, K.D.; Azhar, R.; Ashton-Butt, A.; Lechner, A.M.; Azhar, B. Assessment of ALOS-2 PALSAR-2L-band and Sentinel-1 C-band SAR backscatter for discriminating between large-scale oil palm plantations and smallholdings on tropical peatlands. *Remote Sens. Appl. Soc. Environ.* **2019**, *13*, 183–190. [[CrossRef](#)]
65. Sarzynski, T.; Giam, X.; Carrasco, L.; Lee, J.S.H. Combining Radar and Optical Imagery to Map Oil Palm Plantations in Sumatra, Indonesia, Using the Google Earth Engine. *Remote Sens.* **2020**, *12*, 1220. [[CrossRef](#)]
66. Wagner, M.; Wentz, E.A.; Stuhlmacher, M. Quantifying oil palm expansion in Southeast Asia from 2000 to 2015: A data fusion approach. *J. Land Use Sci.* **2022**, *17*, 26–46. [[CrossRef](#)]
67. Xu, K.; Qian, J.; Hu, Z.; Duan, Z.; Chen, C.; Liu, J.; Sun, J.; Wei, S.; Xing, X. A New Machine Learning Approach in Detecting the Oil Palm Plantations Using Remote Sensing Data. *Remote Sens.* **2021**, *13*, 236. [[CrossRef](#)]
68. Lillesand, T.; Kiefer, R.W.; Chipman, J. *Remote Sensing and Image Interpretation*; John Wiley & Sons: Hoboken, NJ, USA, 2015.
69. Danylo, O.; Pirker, J.; Lemoine, G.; Ceccherini, G.; See, L.; McCallum, I.; Hadi; Kraxner, F.; Achard, F.; Fritz, S. A map of the extent and year of detection of oil palm plantations in Indonesia, Malaysia and Thailand. *Sci. Data* **2021**, *8*, 96. [[CrossRef](#)] [[PubMed](#)]
70. MapBiomass Indonesia. Collection 2 time-series maps of land-use and land-cover. 2022. Available online: <https://mapbiomas.nusantara.earth> (accessed on 21 November 2022).
71. Olofsson, P.; Foody, G.M.; Herold, M.; Stehman, S.V.; Woodcock, C.E.; Wulder, M.A. Good practices for estimating area and assessing accuracy of land change. *Remote Sens. Environ.* **2014**, *148*, 42–57. [[CrossRef](#)]
72. Diek, S.; Fornallaz, F.; Schaepman, M.E.; De Jong, R. Barest Pixel Composite for Agricultural Areas Using Landsat Time Series. *Remote Sens.* **2017**, *9*, 1245. [[CrossRef](#)]
73. Verbesselt, J.; Hyndman, R.; Zeileis, A.; Culvenor, D. Phenological change detection while accounting for abrupt and gradual trends in satellite image time series. *Remote Sens. Environ.* **2010**, *114*, 2970–2980. [[CrossRef](#)]
74. Martin, A.; Osswald, C. A new generalization of the proportional conflict redistribution rule stable in terms of decision. *arXiv* **2008**, arXiv:0806.1797.
75. Smarandache, F.; Dezert, J. Information fusion based on new proportional conflict redistribution rules. In Proceedings of the 2005 7th International Conference on Information Fusion, Philadelphia, PA, USA, 25–28 July 2005; Volume 2, p. 8. [[CrossRef](#)]
76. Gramm, J.; Guo, J.; Hüffner, F.; Niedermeier, R.; Piepho, H.P.; Schmid, R. Algorithms for compact letter displays: Comparison and evaluation. *Comput. Stat. Data Anal.* **2007**, *52*, 725–736. [[CrossRef](#)]
77. Indonesian Ministry of Agriculture *Tree Crop Estate Statistics Of Indonesia 2018-2020-Palm Oil*; Directorate General of Estate Crops Jakarta, Indonesia, 2023. Available online: <https://ditjenbun.pertanian.go.id/?publikasi=buku-publikasi-statistik-2018-2020> (accessed on 29 December 2024)

78. Descals, A.; Wich, S.; Szantoi, Z.; Struebig, M.J.; Dennis, R.; Hatton, Z.; Ariffin, T.; Unus, N.; Gaveau, D.L.A.; Meijaard, E. High-resolution global map of closed-canopy coconut palm. *Earth Syst. Sci. Data* **2023**, *15*, 3991–4010. [[CrossRef](#)]
79. Arvor, D.; Betbeder, J.; Daher, F.R.G.; Blossier, T.; Roux, R.L.; Corgne, S.; Corpetti, T.; Silgueiro, V.d.F.; Junior, C.A.d.S. Towards user-adaptive remote sensing: Knowledge-driven automatic classification of Sentinel-2 time series. *Remote Sens. Environ.* **2021**, *264*, 112615. [[CrossRef](#)]
80. Schumaker, N.H. Using Landscape Indices to Predict Habitat Connectivity. *Ecology* **1996**, *77*, 1210–1225. [[CrossRef](#)]
81. Shen, H.; Lin, Y.; Tian, Q.; Xu, K.; Jiao, J. A comparison of multiple classifier combinations using different voting-weights for remote sensing image classification. *Int. J. Remote Sens.* **2018**, *39*, 3705–3722. [[CrossRef](#)]
82. Wang, X.; Xu, M.; Xiong, X.; Ning, C. Remote Sensing Scene Classification Using Heterogeneous Feature Extraction and Multi-Level Fusion. *IEEE Access* **2020**, *8*, 217628–217641. [[CrossRef](#)]

Disclaimer/Publisher’s Note: The statements, opinions and data contained in all publications are solely those of the individual author(s) and contributor(s) and not of MDPI and/or the editor(s). MDPI and/or the editor(s) disclaim responsibility for any injury to people or property resulting from any ideas, methods, instructions or products referred to in the content.